NRJ THE NEURORADIOLOGY JOURNAL

Neuroradiol J. 2024 Nov 25:19714009241303065. Online ahead of print. doi: 10.1177/19714009241303065

Association of imaging biomarkers with molecular subtypes of medulloblastoma

Maryam Aljaafary [1,2,✉], Akeel A Alali [3,4]

Author information Copyright and License information

PMCID: PMC11590077 PMID: 39586576

Abstract

Background and purpose: The World Health Organization (WHO) subdivided medulloblastoma into genetic and histopathological groups, each with a specific therapeutic intervention and different clinical outcomes. These subtypes may present with distinct imaging features. Therefore, the current study aimed to identify magnetic resonance imaging (MRI) biomarkers to predict the precise pathological characteristics of medulloblastoma. **Methods:** This study included 28 patients with a first diagnosis of medulloblastoma who underwent preoperative brain MRI with subsequent surgical resection and histopathological confirmation at our hospital between 2010 and 2022. Conventional MRI parameters, including apparent diffusion coefficient (ADC) mean values, were correlated with molecular subtypes to identify distinct MRI biomarkers. **Results:** Out of 28 tumors, two (7.1%) tumors exhibited wingless (WNT) activation, thirteen (46.4%) exhibited sonic hedgehog (SHH) activation, and thirteen (46.4%) exhibited non-WNT/non-SHH activation (Group 3 or 4). Statistical analysis revealed a significant association of SHH-activated tumors with paramidline/cerebellar location and the presence of peritumoral edema (p value = <0.0001). No significant correlations were found between the genetic subtypes and the other MRI parameters. A distinctive distribution of the ADC-mean values among the various genetic subtypes with recognizable tendencies was identified. However, it was statistically insignificant. **Conclusion:** Conventional MRI features of the paramidline/hemispheric location and the presence of peritumoral edema were significantly correlated with the SHH activated pathway and hence can be used to facilitate the preoperative implementation of SHH-targeted therapeutic intervention. Although the ADC-mean measurements were not statistically significant, a recognizable distribution of values among the various genetic subtypes was identified.

Keywords: Medulloblastoma, posterior fossa tumor, molecular subgroups, apparent diffusion coefficient

Background and purpose

Medulloblastoma is a malignant primary brain tumor of embryonal origin.[1] It is the most common malignant brain neoplasm in children, accounting for nearly 20% of all pediatric brain tumors.[2] In contrast, the tumors rarely occur in adults, making up only 1% of adult brain tumors.[3] The 2021 revision of the World Health

Organization (WHO) Classification of Tumors of the Central Nervous System categorized medulloblastoma as WHO grade IV due to its rapid disease course, aggressive behavior, and inevitable fatal outcome if not treated with multimodal therapeutic interventions. Given their clinical and biological heterogeneity, the WHO classification divides tumors into molecular and histopathological groups. The four molecular subgroups were wingless (WNT)-activated, sonic hedgehog (SHH)-activated, and non-WNT/non-SHH (Group 3 or 4). The histopathological subgroup is composed of one inclusive generic term known as *Medulloblastoma, histologically defined,* which combines four histological types: classic, desmoplastic/nodular, medulloblastoma with extensive nodularity (MBEN), and large cell/anaplastic.[4,5]

Various prognostic factors that aid in predicting patient outcomes have been identified. These data included patient age, stage, extent of residual disease after surgery, presence or absence of metastasis, histological and molecular subtypes, and rapid implementation of targeted multimodal therapies.[2,6,7] In particular, various medulloblastoma subgroups are linked to markedly distinct survival outcomes. For instance, desmoplastic/nodular and medulloblastoma with extensive nodularity histologic subtypes are associated with a good prognosis, while the classic and large cell/anaplastic subtypes are usually indicative of a poor prognosis.[6] The WNT-activated molecular subtype has an excellent prognosis due to its lack of a functional blood brain barrier, which facilitates the penetration of systemic chemotherapy.[8] In contrast, the Group 3 subtype is associated with a poor prognosis due to its marked propensity to metastasize.[9] Numerous novel therapeutic agents are being tested to target certain specific subtypes to maximize efficacy.[3,8,10]

The extent of surgical resection and the benefit of performing another surgery for residual tumors can be significantly altered based on the provided molecular subgroup.[11] For instance, few studies have reported no significant survival benefit of complete resection over incomplete resection in patients with WNT and SHH tumors. Furthermore, surgical resection of small residual tumoral components is not recommended for these molecular subtypes when the risk of postsurgical morbidity is high. In contrast, disease progression was significantly associated with incomplete resection of non-SHH/non-WNT tumors compared with complete surgical resection. Therefore, the preoperative prediction of the molecular subtype of medulloblastoma could influence the selection of a molecular-based surgical approach.[11,12]

Certain magnetic resonance imaging (MRI) biomarkers can be used to predict the histologic and molecular subtypes of medulloblastoma and can be particularly utilized when the genetic profile is not available. These included location, peritumoral edema, hydrocephalus, enhancement, cyst, margin, drop metastasis, hemorrhage and mineralization.[5,7]

The apparent diffusion coefficient (ADC) is a quantitative MRI parameter that correlates with tumor cellular density and has emerged as a useful tool for characterizing brain neoplasms.[5,13–15] The use of ADC values for distinguishing between medulloblastoma and other posterior fossa neoplasms has been illustrated in many studies.[13–15] The ADC cutoff value of 660 mm2/s was a good indicator of ependymoma. Moreover, a cutoff value between 700 and 900 mm2/s can be utilized to distinguish medulloblastoma from pilocytic astrocytoma.[16] Additionally, the use of ADC maps was found to be highly valuable for determining the infiltrative pattern of the tumor; hence, these maps can be utilized in preoperative planning for safe and adequate resection of medulloblastoma.[17] Moreover, the application of ADC values in providing accurate histopathological classification of medulloblastomas has been well established in many studies.[5,18] Only a

few studies have reported the utility of calculated ADC values in accurately predicting the molecular subtype of medulloblastoma.[7,19] Therefore, it remains substantially underrepresented in the literature.

The preoperative identification of the molecular subtype of medulloblastoma is crucial for determining the extent of surgical resection, facilitating the preoperative implementation of targeted molecular pathway therapies, and predicting prognostic outcomes.[3,8,10–12] Therefore, the aim of the current study was to identify certain MRI biomarkers, with particular emphasis on calculating ADC values, for predicting precise molecular subtypes of medulloblastoma.

Methodology

Patient data

This retrospective single-center analysis included patients with a first diagnosis of medulloblastoma who underwent preoperative brain MRI with subsequent surgical resection and histopathological confirmation at our hospital from 2010 to 2022. Prior to data collection, ethical approval for this study was granted by our local institutional review board with a waiver of consent.

Imaging protocol

The images were obtained using three different MR scanners with different field strengths. Out of 28 patients, only four patients were scanned with a 1.5 T Espree (Siemens), and two were scanned with a 3T Achieva (Philips Health care) MRI scanner. The remaining selected patients were scanned by a 3T Discovery (GE Healthcare) scanner. The preoperative MRI parameters included T1-weighted (sagittal plane, 4 mm slice thickness, 5 mm slice spacing), T2-weighted (axial and coronal planes, 4 mm slice thickness, 5 mm slice spacing), fluid attenuated inversion recovery (FLAIR) [axial plane, 4 mm slice thickness, 5 mm slice spacing], contrast-enhanced T1-weighted sequences (axial and coronal planes, 1 mm slice thickness, 1 mm slice spacing), and susceptibility weighted images (SWI) [axial plane, 3 mm slice thickness, 1 mm slice spacing].

Diffusion-weighted imaging (DWI) sequences were acquired in three orthogonal directions and the following parameters were obtained: 4 mm slice thickness, 5 mm slice spacing, repetition time ms/echo time ms (TR/TE): 5800.00/107.00 ms (1.5 T) and 7750.00/79 ms (3 T). The corresponding ADC values were generated from b0 and b1000 data. The majority of the selected patients (23 out of 28 patients) had prior preoperative brain computed tomography (CT) scans.

Histopathology confirmation

The diagnosis of medulloblastoma was neuropathologically established at the Department of Neuropathology by two experienced neuropathologists with more than 8 years of experience. The tumors were categorized based on the WHO Classification of Tumors of the Central Nervous System (2016).

Imaging criteria definition and analysis

The MRI parameters were analyzed blindly and irrespective of the histologic and genetic subtypes of the patients by a senior radiology resident under the supervision of a neuroradiology consultant with 6 years of experience. The conventional MRI parameters are location (midline or cerebellar hemisphere), the presence or absence of edema (using T2WI/FLAIR sequences), hydrocephalus (defined as widening of the supratentorial ventricles due to infratentorial mass), drop metastasis (defined as neoplasm spread inferiorly along the cerebrospinal spaces), cysts (none, small ≤1 cm, large >1 cm), margin (ill-defined or well-defined), the presence or absence of hemorrhage and mineralization (using SWI sequence) and tumor signal intensity (Using T2WI sequence: hypointense, isointense, hyperintense or heterogeneous to gray matter). Contrast enhancement was characterized (based on Perreault et al. [19]) as solid (if 90% of the tumor volume was estimated to be enhanced), heterogeneous (if the degree of tumor enhancement ranged from 10% to 90%), or minimal (if <10% of the tumor volume was estimated to be enhanced).

Quantitative ADC analysis

The ADC measurements were calculated for each preoperative MRI. The regions of interest (ROIs) were placed within the solid component of the tumor, avoiding regions of inhomogeneity such as necrosis, mineralization, hemorrhage or cysts. To avoid discrepancies within the measured values, the ROIs were placed thrice in each patient, and the results of the ROI calculations were averaged (Figure 1).

Figure 1.

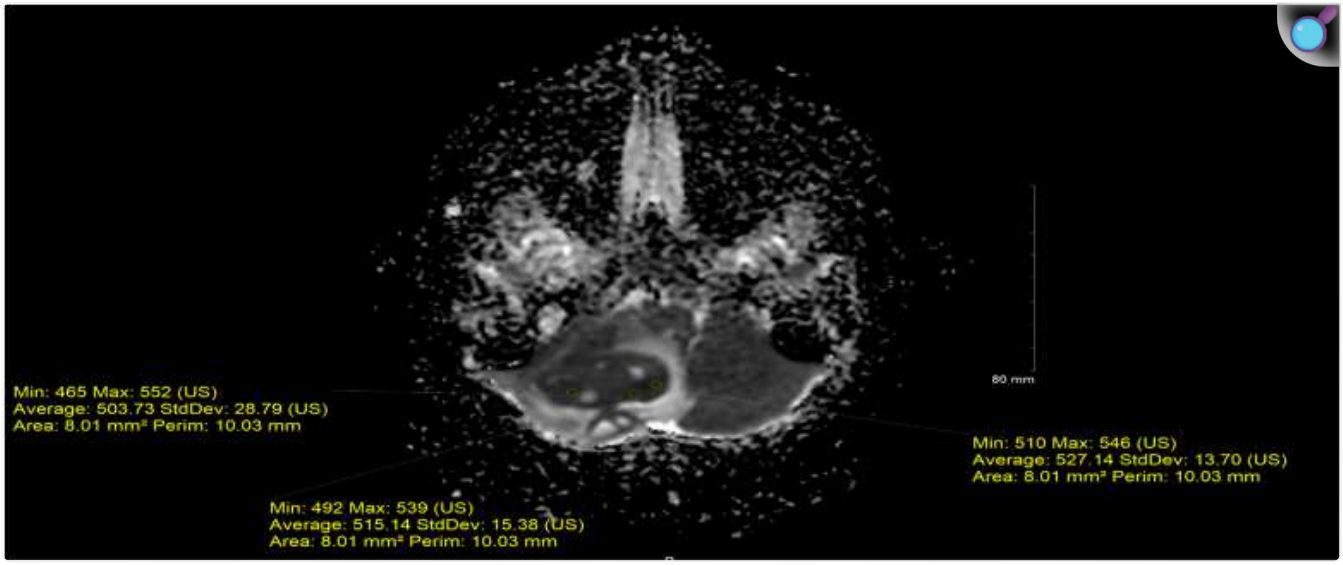

Open in a new tab

Apparent diffusion coefficient (ADC) measurement of medulloblastoma. In each patient, three regions of interest (ROI) were manually placed within the solid component of the tumor avoiding regions of inhomogeneity such as necrosis, mineralization, hemorrhage, or cysts. Then, the results of these measurements were averaged.

Statistics

The statistical data were analyzed using the Statistical Package for the Social Sciences (SPSS). Because of the general assumption regarding the relationship between MRI parameters, histological and genetic subtypes could not be determined. Therefore, an exploratory statistical approach was implemented to test MRI parameters against all histopathological and genetic subtypes to identify possible MRI biomarkers. A p value <.05 was considered to indicate statistical significance.

Results

The demographic data and genetic and histopathological classification of the study population are presented in Table 1. Nine of 28 patients (32%) were female. Seven of 28 patients (25%) were adults. The median patient ages at diagnosis for the pediatric and adult age groups were 5 years (range, 1–11 years) and 22 years (range, 17–33 years), respectively.

Table 1.

Cohort demographics.

	Patient's age group	
	Adult *n* = 7	**Pediatric *n* = 21**
Median age (range in years)	22 (17–33)	5 (1–11)
Gender (no.) (%)		
Male	6 (85.7%)	13 (61.9%)
Female	1 (14.3%)	8 (38.1%)
Genetic subtypes (no.) (%)		
WNT	0 (0.0%)	2 (9.5%)
SHH	5 (71.4%)	8 (38.1%)
Non-WNT/non-SHH	2 (28.6%)	11 (52.4%)
Histopathology subtypes (no.) (%)		
Classic	1 (14.3%)	9 (42.9%)
Desmoplastic/nodular	5 (71.4%)	11 (52.4%)
Large cell anaplastic	1 (14.3%)	1 (4.8%)

Open in a new tab

Neuropathology

The results of MRI parameters with genetic and histological subtypes are illustrated in Table 2. Among the 28 tumors, two (7.1%) tumors showed WNT activation and manifested only in the pediatric population; thirteen (46.4%) were SHH activated, and thirteen (46.4%) were classified as non-WNT/non-SHH (Group 3 or 4). Among the 28 tumors, ten (35.7%) were categorized as classic, sixteen (57.1%) as desmoplastic/nodular, and two (7.1%) as large cell/anaplastic, these patients exclusively exhibited a non-WNT/non-SHH (Group 3 or 4) genetic subtype with significant statistical correlation (p value <.0001). The majority of desmoplastic/nodular subtypes were significantly associated with SHH pathway activation (p value <.0001). The presence of the classic subtype was statistically significant among the non-WNT/non-SHH (group 3 or 4) subtypes (p value = <0.0001).

Table 2.

Conventional MRI parameters with genetic and histological subtypes.

	Genetic subtypes				
	WNT (*n* = 2)	**SHH (*n* = 13)**	**Non-WNT/non-SHH (*n* = 13)**	***p* value**	
Histopathology subtypes					
Classic	2	0	8	<.0001	Fisher's Exact Test
Desmoplastic/nodular	0	13	3		
Large cell anaplastic	0	0	2		
Location (midline/hemispheric)	2/0	2/11	12/1	<.0001	Fisher's Exact Test
Edema (n)	1	13	3	<.0001	Fisher's Exact Test
Hydrocephalus (n)	2	12	13	.55	Chi-square test
T2SI	2	13	13	.577	Fisher's Exact Test
Enhancement (heterogenous/minimal/solid)	0/1/1	8/2/3	3/4/6	.187	Fisher's Exact Test
Cysts (none/small/large)	0/2/0	1/7/5	4/8/1	.235	Fisher's Exact Test
Hemorrhage/mineralization (n)	1	5	8	.706	Fisher's Exact Test
Margin (ill-defined/well-defined)	0/2	1/12	0/13	.55	Chi-square test
Drop metastasis	0	0	1	.55	Chi-square test

Open in a new tab

Analysis of conventional MRI parameters and ADC values

Illustrations of the distinct MRI parameters according to the medulloblastoma molecular subgroups are presented in Figures 2–6. Table 2 provides further information regarding the associations between MRI

parameters and genetic subtypes. Statistical analysis revealed a significant difference in tumor location between the various genetic subtypes (*p* value <.0001). Furthermore, SHH-activated tumors were significantly located in the paramidline/cerebellar hemisphere (*n* = 11/13, 84.6%), while WNT and non-WNT/non-SHH (Group 3 or 4) medulloblastomas were significantly more frequently located in the midline/cerebellar vermis (*n* = 2/2, 100% and 12/13, 92.3%, respectively) (Figure 2).

Figure 5.

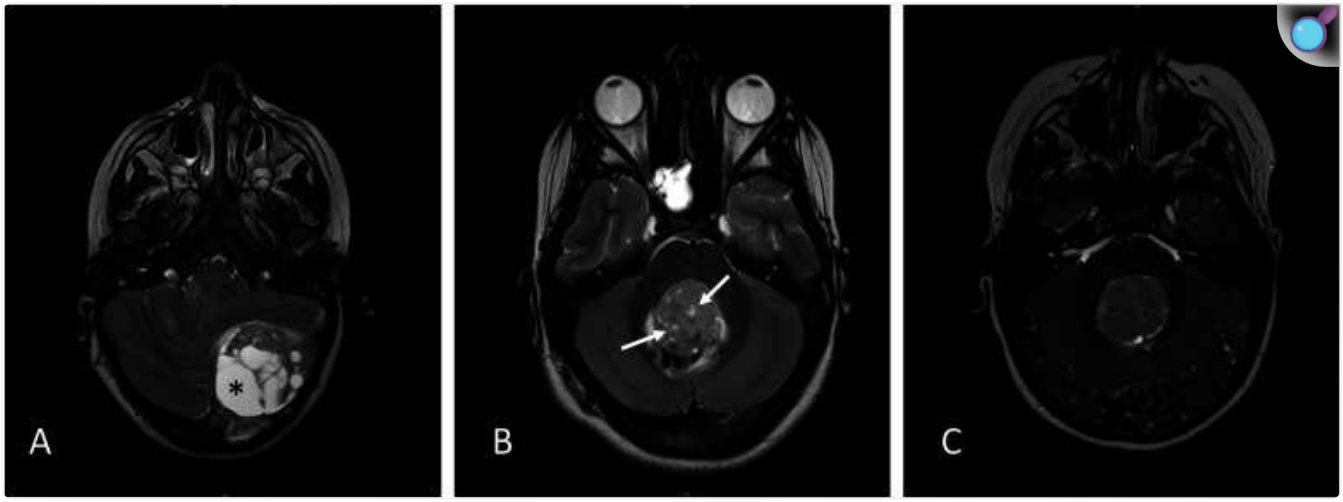

Open in a new tab

Illustration of the presence and absence of large or small cysts (macro/microcystic appearance) in distinct medulloblastoma molecular subgroups using T2-weighted imaging. (A) SHH subtype demonstrates numerous large cysts (asterisk), measuring >1 cm, (B) WNT subtype shows small cysts (arrows), measuring <1 cm, and (C) non-WNT/non-SHH subtype shows complete solid appearance of the tumor without cystic components.

Figure 2.

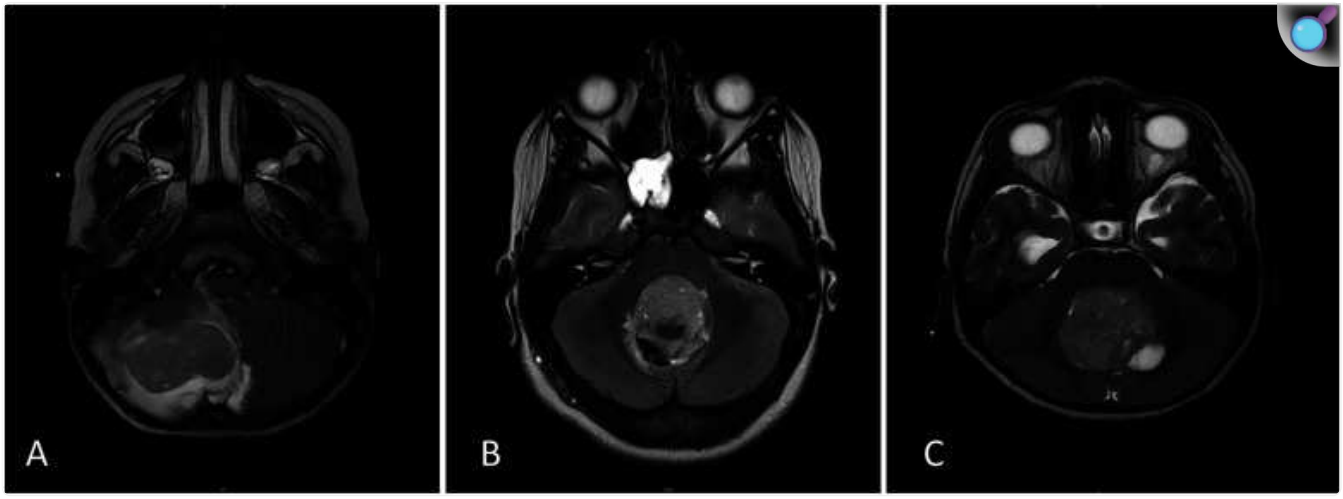

Open in a new tab

Characteristic locations of different medulloblastoma molecular subgroups in T2-weighted images. (A) SHH subtype with para-midline/cerebellar hemisphere location. (B) WNT and (C) Non-WNT/non-SHH subtypes with midline/cerebellar vermis location.

Figure 6.

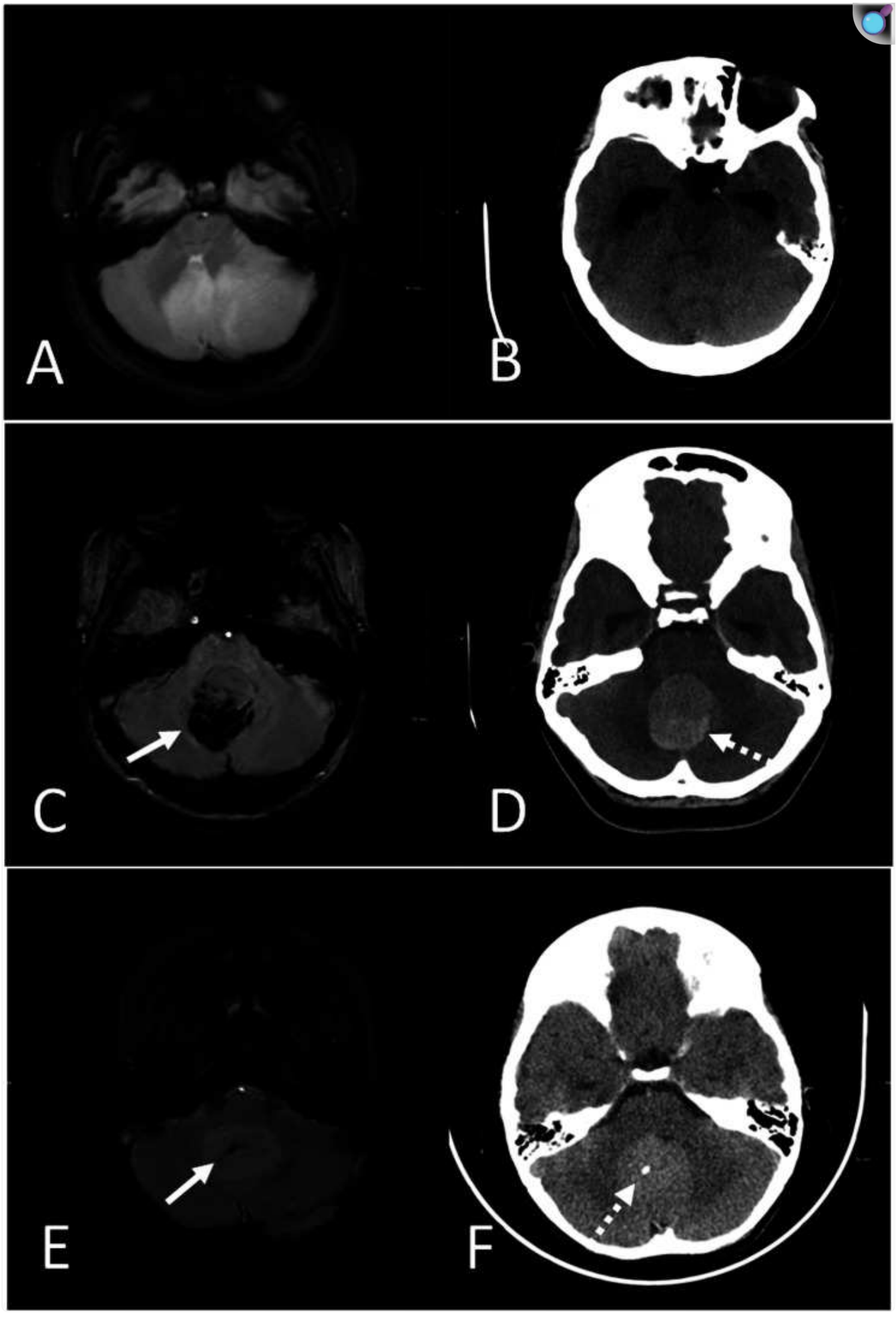
A
B
C
D
E
F

Open in a new tab

Illustration of the presence and absence of hemorrhage and/or mineralization in distinct medulloblastoma molecular subgroups using SWI and unenhanced CT scan. SWI (A) and brain CT (B) images of SHH subtype demonstrate no intra-tumoral hemorrhage nor mineralization. SWI image (C) of WNT subtype shows susceptibility artifact (arrow), corresponding to the marked intrinsic hemorrhagic component (dashed arrow) on unenhanced brain CT (D). SWI (E) of Non-WNT/non-SHH subtype shows a central focus of susceptibility artifact (arrow) corresponding to the intra-tumoral calcification (dashed arrow) noted on unenhanced brain CT (F).

Compared with those of the other subtypes, peritumoural edema was predominantly observed in the SHH-activated medulloblastomas (n = 13/17, 76.4%), and this difference was statistically significant (p value <.0001) (Figure 3).

Figure 3.

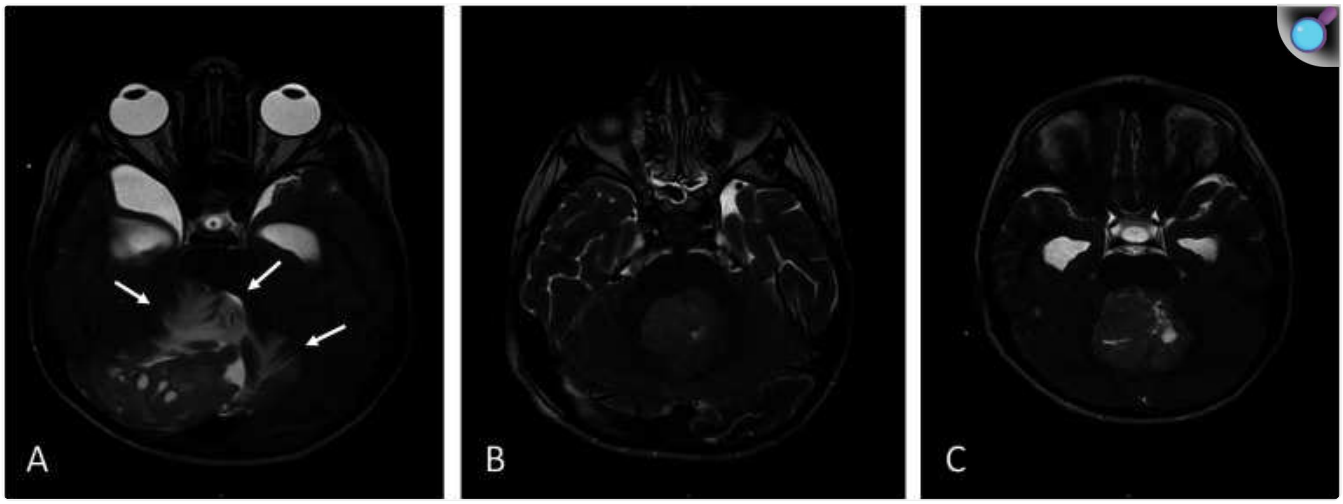

Open in a new tab

Illustration of the presence or absence of edema in various medulloblastoma molecular subgroups using T2-weighted images. (A) SHH subtype demonstrates marked peritumoral edema (arrows). Meanwhile (B) WNT and (C) non-WNT/non-SHH subtypes show no appreciative surrounding edema.

No significant associations were found between the genetic subtypes and the other MRI parameters, including hydrocephalus, tumoral T2WI signal intensity and margin, contrast enhancement, cyst formation, hemorrhage or calcifications and drop metastasis (p value >.05, for any of the abovementioned parameters) (Figures 4–6).

Figure 4.

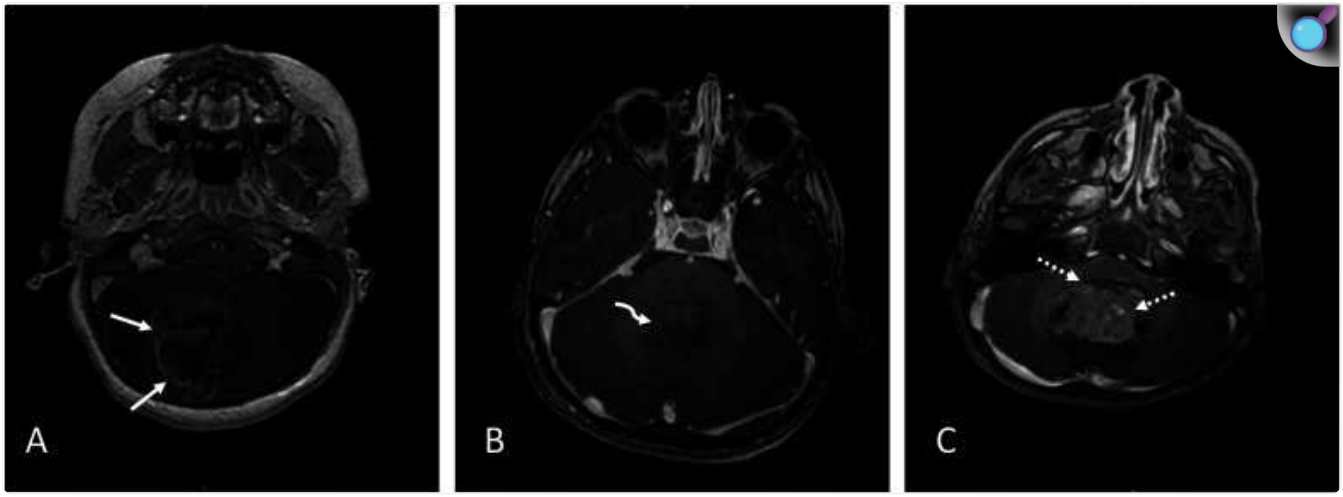

Open in a new tab

Illustration of different enhancement patterns in various medulloblastoma molecular subgroups using T1 post contrast imaging. (A) SHH subtype shows heterogenous enhancement (arrows), (B) WNT subtype shows minimal enhancement (curved arrow) and (C) non-WNT/non-SHH subtype shows solid enhancement (dashed arrows).

The results of the quantitative ADC analysis are shown in Table 3. The calculated ADC-mean (10−6 mm2/s) was 551.5 ± 105.35 (395.11–1498.11 at 95% CI) for WNT-activated, 617 ± 76.9 (570.52–663.48 at 95% CI) for SHH-activated, and 626.38 ± 133.29 (545.84–706.93 at 95% CI) for non-WNT/non-SHH medulloblastoma. These values were not considered to be statistically significant for different genetic subtypes (*p* value = .667).

Table 3.

Quantitative ADC analysis.

	Genetic subtypes			
	WNT (*n* = 2)	**SHH (*n* = 13)**	**Non-WNT/non-SHH (*n* = 13)**	***p* value**
ADC mean (10−6 mm^2/s) ± SD (95% CI)	551.5 ± 105.35 (395.11–1498.11)	617 ± 76.9 (570.52–663.48)	626.38 ± 133.29 (545.84–706.93)	.667

Open in a new tab

Discussion

In the current study, we investigated the possible correlation between neuropathological subtypes of medulloblastoma and several conventional MRI parameters (including quantitative ADC) in both adult and pediatric populations to obtain precise pathological information without relying on invasive intervention to implement targeted regimens.

Two conventional MRI parameters were identified in this study to facilitate the detection of the SHH-activated pathway among other subtypes in terms of the paramidline/hemispheric location and the presence of peritumoral edema. Several studies that aimed to identify potential MRI biomarkers of medulloblastoma reported similar positive findings,[7,19] further augmenting the distinctive biomarkers of SHH-activated pathway tumors in relation to the others. Nevertheless, there was no significant difference between the WNT and non-WNT/non-SHH subtypes in terms of location, as they both preferred midline/cerebellar vermis locations. The abovementioned observation was confirmed by many studies,[7,19,20] rendering it practically impossible to distinguish both entities based solely on their anatomical location.

Moreover, the distinctive presence of peritumoral edema on SHH-activated pathway tumors was similarly illustrated in previous studies. For instance, Reis et al. [7] and Keil et al. [21] reported peritumoral edema to be a highly specific marker for SHH subtypes. In contrast, Yeom et al. [5] and Perreault et al. [19] revealed no obvious associations between the presented MRI parameter and any neuropathological subtypes, including pathologically proven SHH tumors.

The remaining conventional MRI parameters did not show any statistically significant associations with any genetic subtypes. The current findings contrast with those of a few other authors[19,21] who reported a highly significant difference between non-WNT/non-SHH (Group 3 or 4), particularly Group 4, and other genetic subtypes in terms of the minimal enhancement pattern and the presence of intrinsic hemorrhagic component.

The current study did not identify any significant difference between genetic subtypes in terms of varied ADC-mean values within the solid tumoral components, which is likely attributed to the small sample size, primarily in the WNT-activated pathway (n = 2). Nonetheless, there was a distinctive distribution of the mean ADC values among the various genetic subtypes, with the highest and lowest ADC values observed in the non-WNT/non-SHH (626.38 ± 133.29) and WNT (551.5 ± 105.35) subtypes, respectively. The aforementioned observation is concordant with many authors[7,22] who reported equivalent findings.

The advantages of incorporating this information into the clinical domain are numerous. The four molecular subgroups have shown distinct clinical behaviors and prognostic outcomes; therefore, multimodal therapeutic interventions are being tailored to target a specific molecular activated pathway to maximize efficacy.[8,19] Identifying such MRI biomarkers could further assist and reinforce the radiopathological interpretations of the molecular analysis of medulloblastoma. It could play a key role in molecular classification when access to genetic stratification is not feasible and may enable immediate initiation of personalized treatments while awaiting surgical resection and histopathology results. [19] Furthermore, artificial intelligence in neuroradiology is considered a promising technology, for the precise differentiation

of medulloblastoma mimics and their genetic subtypes through the incorporation of clinical, molecular and radiomic markers extracted from conventional MRI parameters. Recognizing the MRI features of molecular subgroups might provide insight into these endeavors to improve patient outcome. [23]

Conclusion

Conventional MRI features of the paramidline/hemispheric location and the presence of peritumoral edema were significantly correlated with the SHH-activated pathway; and therefore, they can be used to facilitate the preoperative implementation of SHH-targeted therapeutic intervention and to predict clinical outcomes. A distinctive distribution of the ADC-mean values among the various genetic subtypes with recognizable tendencies was identified. Nevertheless, it remains statistically insignificant.

Further confirmation of the validated imaging features is advised through the implementation of an international multicenter study with an adequate sample size to properly construct a reliable MRI-based diagnostic algorithm. As a result, the use of MRI biomarkers for the preoperative identification of the molecular subtype could facilitate the preoperative implementation of targeted molecular pathway therapies, determine the extent of surgical resection, minimize postoperative deficits, and predict the prognostic outcome. Furthermore, the incorporation of additional quantitative MRI studies, such as MRI perfusion and spectroscopy, might add a novel perspective to the current understanding of radiopathological analysis of medulloblastoma.

Limitations

The major limitation of the present study was attributed to the small patient cohort and the nonuniform distribution of data across different neuropathological subtypes, particularly in WNT-activated tumors, which might have negatively impacted the accurate identification of potential biomarkers. Further validation of these MRI-based molecular stratifications through the implementation of a multicentric study with an adequate sample size is crucial for predicting its accuracy and feasibility.

Since preoperative brain CT was not performed on all selected patients, the present study was additionally limited by the lack of independent statistical analysis of hemorrhage and mineralization. As a consequence, the inclusion of these conventional parameters as potentially useful tools in the preoperative molecular-based stratification of medulloblastoma was adversely affected by the present limitations.

The mean ADC values of the ROIs were calculated, and the ROIs were placed within the solid component of the tumor on each preoperative MRI to avoid regions of inhomogeneity to the greatest extent. Nonetheless, microscopic intra-tumoral variation, including imperceptible necrosis on imaging, may have marginally altered the analysis of the ADC values. Providing ADC values with full precision could be achieved through concomitant utilization of MR spectroscopy and/or perfusion, which might aid in more accurate placement of ROIs within the solid components of the tumor.

Footnotes

Author contributions: MA contributed to the study conception and design, data acquisition, analysis, interpretation, and writing of the article. AA contributed in editing, reviewing of the article and approved the final version of the article.

The author(s) declared no potential conflicts of interest with respect to the research, authorship, and/or publication of this article.

Funding: The author(s) received no financial support for the research, authorship, and/or publication of this article.

ORCID iDs

Maryam Aljaafary https://orcid.org/0009-0003-5860-1108

Akeel A Alali https://orcid.org/0000-0003-4619-7489

References

1. Eibl T, Hammer A, Yakubov E, et al. Medulloblastoma in adults - reviewing the literature from a surgeon's point of view. Aging (Albany NY) 2021; 13: 3146–3160. [DOI] [PMC free article] [PubMed] [Google Scholar]

2. Mahapatra S, Amsbaugh MJ. Medulloblastoma. Treasure Island, FL: StatPearls Publishing, 2020. https://www.ncbi.nlm.nih.gov/books/NBK431069/. [PubMed] [Google Scholar]

3. Rood BR, Macdonald TJ, Packer RJ. Current treatment of medulloblastoma: recent advances and future challenges. Semin Oncol 2004; 31: 666–675. [DOI] [PubMed] [Google Scholar]

4. Louis DN, Perry A, Wesseling P, et al. The 2021 WHO classification of tumors of the central nervous system: a summary. Neuro Oncol 2021; 23: 1231–1251. [DOI] [PMC free article] [PubMed] [Google Scholar]

5. Yeom KW, Mobley BC, Lober RM, et al. Distinctive MRI features of pediatric medulloblastoma subtypes. AJR Am J Roentgenol 2013; 200: 895–903. [DOI] [PubMed] [Google Scholar]

6. Liu Y, Xiao B, Li S, et al. Risk factors for survival in patients with medulloblastoma: a systematic review and meta-analysis. Front Oncol 2022; 12: 827054. [DOI] [PMC free article] [PubMed] [Google Scholar]

7. Reis J, Stahl R, Zimmermann H, et al. Advanced MRI findings in medulloblastomas: relationship to genetic subtypes, histopathology, and immunohistochemistry. J Neuroimaging 2021; 31: 306–316. [DOI] [PubMed] [Google Scholar]

8. Menyhart O, Győrffy B. Molecular stratifications, biomarker candidates and new therapeutic

options in current medulloblastoma treatment approaches. Cancer Metastasis Rev 2020; 39: 211–233. [DOI] [PMC free article] [PubMed] [Google Scholar]

9. Taylor MD, Northcott PA, Korshunov A, et al. Molecular subgroups of medulloblastoma: the current consensus. Acta Neuropathol 2012; 123: 465–472. [DOI] [PMC free article] [PubMed] [Google Scholar]

10. Suk Y, Gwynne WD, Burns I, et al. Childhood medulloblastoma: an overview. Methods Mol Biol 2022; 2423: 1–12. [DOI] [PubMed] [Google Scholar]

11. Wang Y, Li KK, Xiong J, et al. Differences in the prognostic value of tumor extent of resection among the molecular subgroups of medulloblastoma: a single centre study of 113 cases. Translational Neuroscience and Clinics 2017; 3: 66–73. [Google Scholar]

12. Thompson EM, Hielscher T, Bouffet E, et al. Prognostic value of medulloblastoma extent of resection after accounting for molecular subgroup: a retrospective integrated clinical and molecular analysis. Lancet Oncol 2016; 17: 484–495. [DOI] [PMC free article] [PubMed] [Google Scholar]

13. Payabvash S, Tihan T, Cha S. Differentiation of cerebellar hemisphere tumors: combining apparent diffusion coefficient histogram analysis and structural MRI features. J Neuroimaging 2018; 28: 656–665. [DOI] [PubMed] [Google Scholar]

14. Wang W, Cheng J, Zhang Y, et al. Use of apparent diffusion coefficient histogram in differentiating between medulloblastoma and pilocytic astrocytoma in children. Med Sci Mon Int Med J Exp Clin Res 2018; 24: 6107–6112. [DOI] [PMC free article] [PubMed] [Google Scholar]

15. Koral K, Alford R, Choudhury N, et al. Applicability of apparent diffusion coefficient ratios in preoperative diagnosis of common pediatric cerebellar tumors across two institutions. Neuroradiology 2014; 56: 781–788. [DOI] [PubMed] [Google Scholar]

16. Dangouloff-Ros V, Varlet P, Levy R, et al. Imaging features of medulloblastoma: conventional imaging, diffusion-weighted imaging, perfusion-weighted imaging, and spectroscopy: from general features to subtypes and characteristics. Neurochirurgie 2021; 67: 6–13. [DOI] [PubMed] [Google Scholar]

17. Marupudi NI, Altinok D, Goncalves L, et al. Apparent diffusion coefficient mapping in medulloblastoma predicts non-infiltrative surgical planes. Childs Nerv Syst 2016; 32: 2183–2187. [DOI] [PubMed] [Google Scholar]

18. Fruehwald-Pallamar J, Puchner SB, Rossi A, et al. Magnetic resonance imaging spectrum of medulloblastoma. Neuroradiology 2011; 53: 387–396. [DOI] [PubMed] [Google Scholar]

19. Perreault S, Ramaswamy V, Achrol AS, et al. MRI surrogates for molecular subgroups of medulloblastoma. Am J Neuroradiol 2014; 35: 1263–1269. [DOI] [PMC free article] [PubMed] [Google Scholar]

20. Patay Z, DeSain LA, Hwang SN, et al. MR Imaging characteristics of wingless-type-subgroup

paediatric medulloblastoma. AJNR AmJ Neuroradiol 2015; 36: 2386–2393. [DOI] [PMC free article] [PubMed] [Google Scholar]

21. Keil VC, Warmuth-Metz M, Reh C, et al. Imaging biomarkers for adult medulloblastomas: genetic entities may be identified by their MR imaging radiophenotype. AJNR Am J Neuroradiol 2017; 38: 1892–1898. [DOI] [PMC free article] [PubMed] [Google Scholar]

22. Reddy N, Ellison DW, Soares BP, et al. Pediatric posterior fossa medulloblastoma: the role of diffusion imaging in identifying molecular groups. J Neuroimaging 2020; 30: 503–511. [DOI] [PubMed] [Google Scholar]

23. Abdel Razek AAK, Alksas A, Shehata M, et al. Clinical applications of artificial intelligence and radiomics in neuro-oncology imaging. Insights Imaging 2021; 12: 152. [DOI] [PMC free article] [PubMed] [Google Scholar]

Articles from The Neuroradiology Journal are provided here courtesy of **SAGE Publications**